

## Numerical and Experimental Study on the Ability of Dynamic Roughness to Alter the Development of a Leading Edge Vortex

Christopher D Griffin<sup>1\*</sup>, Wade W Huebsch<sup>1</sup>, Alric P. Rothmayer<sup>2</sup> and Jay P. Wilhelm<sup>3</sup>

<sup>1</sup>Department of Mechanical and Aerospace Engineering, West Virginia University, Morgantown, WV, 26506, USA

<sup>2</sup>Department of Aerospace Engineering, Iowa State University, Ames, IA 50011, USA

<sup>3</sup>Department of Mechanical Engineering, Ohio University, Athens, OH 45701, USA

### Abstract

Both computational fluid dynamics, using two- and three-dimensional commercial flow solvers (FLUENT), and experimental analysis (Particle Image Velocimetry) were used to document the ability of sub-boundary layer oscillating surface perturbations (dynamic roughness) to alter the development of a leading edge vortex (LEV) on an airfoil undergoing dynamic stall. The ability to delay or instigate LEV development can potentially lead to methods that can take advantage of the sustained lift while limiting the consequences associated with the shedding of the vortex. Both computational and experimental results show the ability of dynamic roughness to alter the development of a LEV on a rapidly pitching airfoil. Computational simulations were performed in a Reynolds number range from 25,000 to 50,000 at a reduced frequency of 0.1, while experiments included this range as well as runs up to a Reynolds number of 200,000 and reduced frequencies of 0.1, 0.15, and 0.2. The lift-to-drag ratio was increased by approximately 60% at 15° AOA.

**Keywords:** Numerical; Dynamic Roughness (DR); Leading Edge Vortex (LEV); Computational Fluid Dynamics (CFD); 2D-3D Commercial Flow

### Introduction

The dynamic stall phenomenon has been recognized as an important aerodynamic mechanism for many decades and it continues to generate significant interest in the research community due to the fact that it occurs in many different types of applications. An equal level of interest can be found in pursuing methodologies that have the potential to control dynamic stall; either delaying or quickening the process. The present work investigates the ability of dynamic roughness (DR) flow control to alter the development of the dynamic stall vortex.

Dynamic stall can be a major factor when dealing with helicopter rotor blades, wind turbines, and highly maneuverable military aircraft. In addition, recent approaches mimicking biological flight (biomimetics) have correlated vortex development to the aerodynamics observed in flapping flight and how some biological flyers take advantage of this leading edge vortex [1-3]. Dynamic stall is a term used to describe the complex unsteady flow phenomenon on a wing that occurs from a rapid pitch up to angles of attack that are larger than the static-stall angle for the airfoil. The resulting flow field is quite different than a wing at a static angle of attack or in a quasi-steady-state motion. A key characteristic of dynamic stall is the formation of a vortex near the airfoil leading edge, often referred to as the leading edge vortex (LEV) or simply as the dynamic stall vortex (DSV). The formation of this vortex is the source of sustained lift associated with dynamic stall. Lift is then lost as the vortex sheds into the wake, which then causes an increase in drag as well as a large and often abrupt shift in pitching moment [4].

Previous attempts to alter the LEV development have used strategies similar to laminar boundary layer control methods, including: suction, injection, vortex generators, roughness, compliant surfaces, slats and more recently, techniques such as plasma actuators and synthetic jets [5-10]. A flow control apparatus used to alter the LEV occurring during dynamic stall should be tunable to operate at a variety of conditions, such as various Reynolds numbers (Re) and pitching frequencies. The current study investigates DR as a mechanism to alter development of the LEV. Dynamic roughness can be defined as time dependent,

sub-boundary-layer-height surface perturbations that are tunable in amplitude and frequency. Similar flow control devices have been investigated, particularly “active dimples” developed by Dearing, et al. [11] and “micro balloon actuators” fabricated and tested by Grosjean et al. [12]. The active dimples create cavities on the surface in order to inject vortices into the turbulent boundary layer and reduce skin friction. The micro balloon actuators were developed to maneuver delta wing aircraft, again predominantly in a turbulent flow regime. The dynamic roughness discussed in this work have been predominantly studied in laminar flow instances.

Prior to the current research effort, extensive work was performed to study the effects of dynamic roughness on the leading edge separation bubble of an airfoil at a static angle of attack. The initial work, by Huebsch [13], developed computational simulations for a laminar leading-edge separation bubble. With this approach, dynamic roughness was shown to eliminate the laminar separation bubble on an idealized parabolic leading edge. This research evolved into a combined numerical and experimental approach to study the ability of dynamic roughness to eliminate the leading edge separation bubble developed on a NACA 0012 airfoil. Two-dimensional and three-dimensional numerical simulations were carried out alongside experimental flow visualizations and surface pressure measurements. Both techniques confirmed the ability of distributed dynamic roughness to eliminate the leading edge separation bubble on a NACA 0012 airfoil at a static angle of attack [14]. Short separation bubbles were suppressed at 9.5° angle of attack at a Re=100,000 and long bubbles were suppressed at 12°

**\*Corresponding author:** Griffin GD, Department of Mechanical and Aerospace Engineering, West Virginia University, Morgantown, WV 26506, USA. Tel: (304) 293-3386; E-mail: [cgriffin@mail.wvu.edu](mailto:cgriffin@mail.wvu.edu)

**Received** September 15, 2016; **Accepted** October 20, 2016; **Published** October 30, 2016

**Citation:** Griffin CD, Huebsch WW, Rothmayer AP, Wilhelm JP (2016) Numerical and Experimental Study on the Ability of Dynamic Roughness to Alter the Development of a Leading Edge Vortex. Fluid Mech Open Acc 3: 137. doi: 10.4172/2476-2296.1000137

**Copyright:** © 2016 Griffin CD, et al. This is an open-access article distributed under the terms of the Creative Commons Attribution License, which permits unrestricted use, distribution, and reproduction in any medium, provided the original author and source are credited.

angle of attack at the same Reynolds number. In addition, leading edge suction was increased during actuation, indicated by surface pressure measurements. Dynamic roughness has even been shown to partially suppress deep stall on static airfoils at Reynolds numbers ranging from 25,000 to 97,000 [15]. Stall delay was identified by calculation of the velocity field via particle image velocimetry (PIV).

The previous success of dynamic roughness as a means of leading-edge separation flow control was the impetus to evaluate its capabilities in highly unsteady aerodynamics, specifically the alteration of LEV development.

## Experimental Method

Wind tunnel tests were conducted to experimentally study the effect of dynamic roughness on the development of the leading edge vortex. The analysis method used was Particle Image Velocimetry (PIV), which calculated the velocity field in the area of interest around the airfoil. The pitching motion of the airfoil was created by developing a four-bar linkage system that oscillated the airfoil about its quarter-chord axis. The dynamic roughness elements were created by adhering a latex skin to the leading edge of the airfoil that was machined to create cavities. A pneumatic system then pressurized these cavities to cause the latex in this region to “bulge”. Further details of the fabrication and experimental analysis are provided below.

## Model design and Fabrication

A NACA 0012 airfoil was selected based on its wide use in previous research, specifically the work done by Huebsch et al. [14] and Grager et al. [15]. A chord length of 0.2921 m (11.5 in.) was used to balance between the desire to create a large-scale model and being mindful to minimize the wind tunnel test section blockage. The motivation behind making the model as large as possible was ease of fabrication and increased durability of the dynamic roughness section. For blockage considerations, the focus was on the worst-case scenario; at the highest angle of attack obtained during the pitching motion (40°) there was a blockage of 16%. In addition, previous research indicates significant reductions in blockage effects when studying rapidly pitching airfoils as compared to airfoils at static angles of attack [16]. This provided confidence that test section blockage did not affect the development of the leading edge vortex. All experimental work was conducted in a closed-loop subsonic wind tunnel. The test section has dimensions of 81.3 cm x 114.3 cm (32 in x 45 in) and turbulence intensity (TI) < 0.1%.

The airfoil shape and support were provided by four aluminum ribs that were milled from 12.7 mm (0.5 in.) thick aluminum sheets on a numerically-controlled end milling machine with a resolution of 0.0127 mm (0.0005 in.). The profile for the airfoil was developed using the NACA four-digit equation [17], which was discretized into 141 points with a bias towards the leading edge. Pockets were milled out of each rib to reduce weight and to allow spacing for the appropriate plumbing connections for the dynamic roughness section of the leading edge. A 12.7 mm (0.5 in.) hole with a keyway was milled at the quarter-chord position for shaft alignment of the airfoil ribs. This ensured no twist was present on the airfoil. The skin of the airfoil was constructed using aluminum sheet metal attached to the ribs with countersunk screws, creating a smooth surface.

The dynamic roughness section was installed between the two inner ribs. This location of the airfoil was where the dynamic roughness elements were located, along with the connections to the pneumatic system that made the dynamic roughness elements expand. This section consisted of two separate portions sealed with a rubber O-ring

gasket to mitigate air leakage, as shown in Figure 1. The leading edge portion contained a cavity milled to create the dynamic roughness plenum as well as the holes that made up the individual dynamic roughness elements. The dynamic roughness elements had a diameter of 5.84 mm (2% chord length) and a span-wise spacing of 8.53 mm (~1.5 diameters, 2.9% chord length), center-to-center. Spacing between chord-wise rows was 6.35 mm (~1.09 diameters, 2.7% chord length), center-to-center. The first row of dynamic roughness elements were located 3.20 mm (~1% chord length) from the leading edge and the last row was located 26.31 mm (~9% chord length) from the leading edge, totaling 53 elements. The general geometry and location of the dynamic roughness elements were based on previous related work and machining capabilities [14,15]. Latex rubber, with a thickness of 0.30 mm, was then adhered to the entire section, allowing the latex above the holes to “bulge” when pressurized while the remaining latex skin remained static and followed the shape of the leading edge. The dynamic roughness section was attached to the plumbing connection block, which was threaded with a 1/8 in. NPT hole to facilitate connection to the pneumatic actuation system. It is important to note the dynamic roughness section was machined to take into account the thickness of the latex rubber. This was to ensure that with no actuation the airfoil would have the profile of a standard “clean” NACA 0012. An assembled model prior to the attachment of the aluminum sheet metal and latex skin is shown in Figure 2. Keyways in the shaft and ribs act to ensure accurate alignment and spacing as well as to prevent slippage while undergoing oscillation during experimentation (Figures 1 and 2).

## Pitching mechanism and Dynamic roughness actuation

A four-bar linkage system was designed and fabricated to oscillate an airfoil between a prescribed minimum and maximum angle of attack, as shown in Figure 3. A 0.373 kW (0.5 hp) variable speed DC

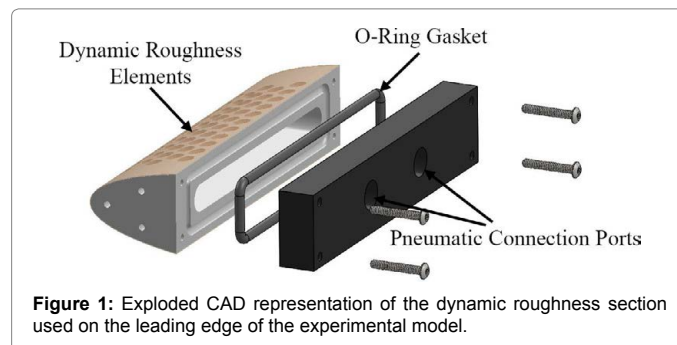


Figure 1: Exploded CAD representation of the dynamic roughness section used on the leading edge of the experimental model.



Figure 2: Assembly of NACA 0012 model with aluminum sheet metal and latex skin removed; the dynamic roughness actuation section is located in the leading edge region of the two center ribs. The shaft through the quarter chord location acts as the rotation axis.



**Figure 3:** Airfoil oscillation mechanism mounted below the wind tunnel test section showing both the four bar linkage as well as the DC motor.

motor was used to drive the system, allowing varying rates of pitch by controlling the motor speed. Similar methods of pitching have been used successfully in previous research [18,19]. An absolute encoder was installed on the end of the shaft to record and display instantaneous angle of attack. The nature of the four-bar mechanism allowed the airfoil to oscillate in a sinusoidal fashion with an angle of attack given by

$$\alpha(t) = \alpha_0 + \alpha_1 \sin(\omega t) \quad (1)$$

Where  $\alpha(t)$  is the instantaneous angle of attack at time  $t$ ,  $\alpha_0$  is the mean angle of attack,  $\alpha_1$  is the oscillation magnitude, and  $\omega$  is the circular frequency. The circular frequency is often non-dimensionalized using Eq. (2) and is termed the reduced frequency,  $k$ .

$$k = \frac{\omega c}{2U_\infty} \quad (2)$$

Here  $c$  is a characteristic length scale, in this case the airfoil's chord length, and  $U_\infty$  is the free-stream velocity. The pitching mechanism was mounted below the test section and was connected to the shaft running through the quarter chord of the airfoil. This shaft was secured at four different locations, two below the test section and two above the test section, to a steel structure that was independent of the test section (Figure 3).

Actuation of the dynamic roughness elements was accomplished using a pneumatic system. A 27 cubic centimeter displacement two-stroke motor was connected via hard plastic tubing to the dynamic roughness plenum in the airfoil. An additional 0.373 kW (0.5 hp) variable speed DC motor drove a belt-pulley system connected to the shaft of the two-stroke motor. The rotation of the DC motor caused the piston inside the two-stroke motor to cycle, thus creating an oscillating pressure source for the dynamic roughness plenum. Both the intake and exhaust ports of the two-stroke motor were covered to create a closed actuation system. The frequency of actuation was controlled by a DC motor controller. A tachometer attached to the DC motor shaft recorded and displayed the instantaneous frequency of the DC motor. High speed video was used to ensure the tachometer reading directly correlated to the dynamic roughness actuation frequency experienced by the model. Before conducting an experimental analysis run, a valve near the piston was opened to ensure the pressure within the piston was equal to the ambient atmospheric pressure. The piston was then manually advanced to its lowest position (bottom-dead-center). The valve was then closed, sealing the actuation system. This ensured a vacuum would not develop within the pneumatic system, therefore creating only positive displacement of the dynamic roughness elements. High speed video was used to confirm cavities, or dimples, did not form. In addition, images were taken of the leading edge in static air as well as during wind tunnel tests to observe any unwanted

displacement of the latex. The images showed no noticeable dimpling or inflation.

Experimental analysis was primarily accomplished using Particle Image Velocimetry (PIV). A commercial PIV system from LaVision, Inc. was used for this research. The system consisted of two Nd:Yag lasers emitting light at a wavelength of 532 nm, a laser arm (allowing easy manipulation of the laser output location), and a variety of optics to produce a laser sheet thickness and focal length optimum for the application. The planar PIV data was collected using an ImagerProX 11 megapixel CCD camera. A programmable timing unit (PTU) and the DAVIS software provided by LaVision, Inc. controlled the synchronization between laser illumination and image capture.

The wing model was mounted vertically in the test section while the laser sheet was illuminated from the side of the test section and the camera was mounted above the test section, as shown in Figure 4. In this scenario a clear wall (i.e., acrylic sheet) was required to allow the laser sheet to enter the test section as well as a clear "roof" that allowed an unimpeded view for the cameras. The absolute encoder was connected to the PTU to trigger laser illumination and image acquisition at prescribed angles of attack during the pitch-up maneuver (Figure 4).

An uncertainty analysis was performed on the PIV setup to quantify the total uncertainty in measured flow velocity, position, and time. A procedure was followed that was developed by the International Towing Tank Conference, and is very in depth in its scope of possible sources of uncertainty in PIV measurements [20]. The error for each possible source was estimated, then a sensitivity calculation was applied to that error. Finally, for each uncertainty type (velocity, position, and time) a root sum square is applied to each uncertainty value to provide a total uncertainty. For all experiments the maximum total uncertainty in velocity was 0.35 m/s, position was 1.09 mm, and time was  $1.00 \times 10^{-8}$  s. Table 1 provides an example of the principal dimensions of the PIV experiment that were used to calculate the uncertainty (Table 1).

## Computational Method

Both two-dimensional and three-dimensional CFD simulations were performed to further study the effect of DR on the development of the LEV. The commercial software Fluent, which utilizes an implicit, finite volume Navier-Stokes solver, was used for all computational studies. A user-defined function (UDF) was developed to simulate

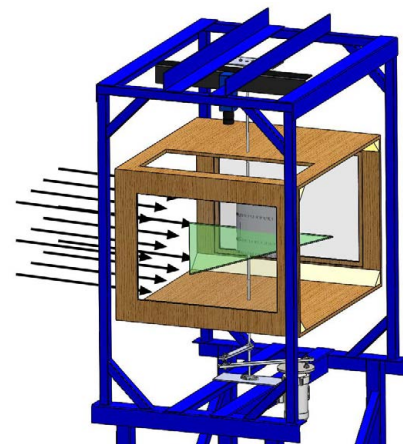


**Figure 4:** Illustration of wind tunnel test section with PIV setup showing laser illumination plane and camera position for planar data collection. Arrows indicate flow direction.

Target flow of measurement	
Target flow	2-D Air Flow
Measurement facility	Closed-Loop Wind Tunnel
Measurement area	460 x 290 mm <sup>2</sup>
Uniform flow speed	10 m/s
Calibration	
Distance of reference points, $L_r$	15 mm
Distance of reference image, $L_i$	150.64 pixels
Magnification factor, $\alpha$	0.09958 mm/pixel
Flow visualization	
Tracer particle	Bis(2-ethylhexyl) sebacate
Average diameter	0.001 mm
Standard deviation of diameter	0.0001 mm
Average specific gravity	0.914
Light source	Double Pulse Nd:YAG laser
Thickness of laser light sheet	1 mm
Time interval	60 $\mu$ s
Image detection	
Camera	
Spatial resolution	4008 x 2672 pixels
Sampling frequency	5 fps
Gray scale resolution	14 bit
Cell size	9 x 9 $\mu$ m <sup>2</sup>
Optical system	
Distance from the target, $L_t$	721.00 mm
Length of focus	62.11 mm
F Number of lens	2.8
Data processing	
Pixel unit analysis	Cross correlation method
Correlation Area Size	16 x 16 pixels

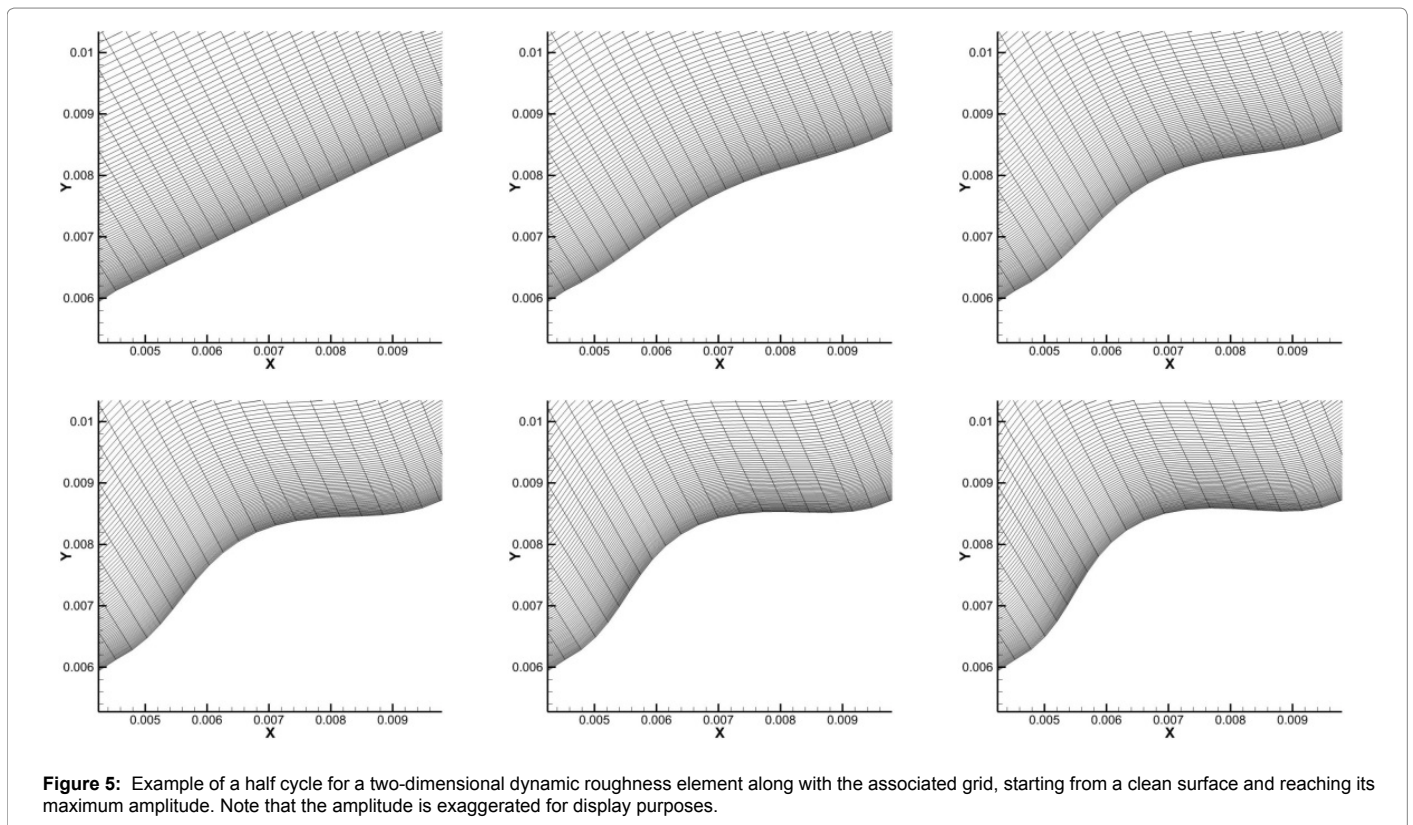
Table 1: Principal dimensions of PIV measurement.

the motion of the dynamic roughness elements utilizing the dynamic meshing capabilities of Fluent. Huebsch et al. [14] developed a predecessor UDF for fixed angle of attack dynamic roughness research. However, the UDF needed for the current effort required the capabilities to not only simulate the motion of the roughness elements, but also to simulate the dynamic pitch-up motion of the airfoil geometry.

In the initial UDF approach used in that work [14], it was thought that re-meshing was required to simulate the motion of the dynamic roughness elements. This approach necessitated an unstructured grid zone consisting of tetrahedral cells in the area of re-meshing. Extensive testing was conducted to determine the dynamic mesh settings needed for adequate re-meshing near the dynamic roughness elements. However, after further development it was found that as long as the grid structure remained adequately orthogonal near the surface of motion, the re-meshing approach was not needed. Instead, only mesh smoothing was needed, which allowed the use of structured, quadrilateral cells, resulting in a more computationally efficient grid in the boundary layer. This alternative approach helped to reduce the complexity of the mesh, which in turn reduced the time needed to reach a converged solution since the algorithms used to remove and replace tetrahedral cells (re-mesh) was no longer needed.

For the dynamic roughness geometry, the UDF created sinusoidal humps with amplitude and frequency that could be set to any desired value. The half-cycle evolution of a single two-dimensional roughness element and a group of three-dimensional roughness elements is shown in (Figures 5 and 6), respectively. Note that the amplitude displayed is exaggerated in the figures as compared to the actual geometries in the simulations to better display surface and mesh motion.

As noted, the UDF also had to simultaneously simulate the pitch up of the airfoil/wing geometry. Initially, a UDF was written to rotate the



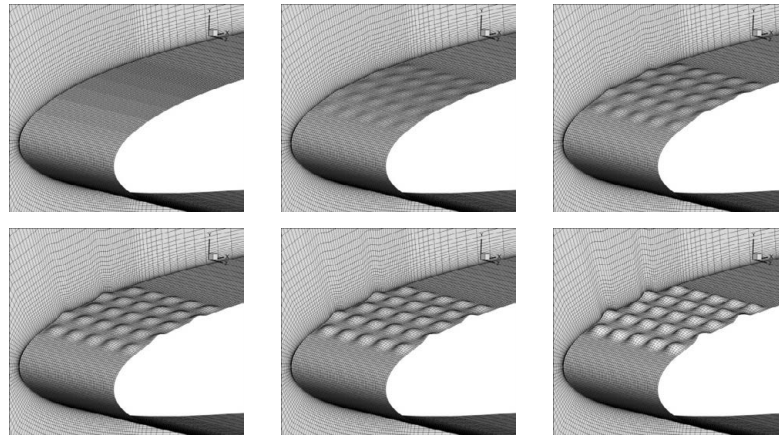


**Figure 6:** Example of a half cycle of a group of simulated three-dimensional dynamic roughness elements, starting from a clean surface and reaching its maximum amplitude. A spanwise slice of the grid is also included. Note that the amplitude is exaggerated for display purposes.

airfoil using a deforming mesh, but the UDF used to create the dynamic roughness elements relied on absolute node position. Therefore, the motion of the nodes that makeup the dynamic roughness elements would become displaced as the airfoil was rotated. This caused poor mesh representation of the dynamic roughness elements. An alternate method was developed that simulated pitching the airfoil while keeping it in the same Cartesian position. This was simply applying a secondary UDF that prescribed a variable velocity inlet condition. Although this method of simulating rapid wing pitch up neglected the inertial terms of the governing equations, the resulting solutions still produced the qualitative trends of separation, reattachment, and recirculation. This approach was deemed sufficient to investigate differences in LEV development between clean and dynamic roughness cases.

The objective of the current effort was to investigate the capability of dynamic roughness to alter the formation of the LEV, which has a laminar separation point. To accurately capture the laminar separation at the leading edge, it was decided to use the laminar flow solver. With this in mind, simulations were done at chord Reynolds numbers less than 150,000. Although it is likely that transition and turbulence occur along the chord at this flow condition, laminar flow still dominates at the separation point in the leading edge region, which is best modeled by the laminar flow solver. Huebsch et al. used a similar approach in their work [14]. The authors acknowledge that the laminar solver may not adequately capture the turbulent and unsteady flow farther downstream on the airfoil, but it is assumed that the laminar separation point is the critical issue in analyzing the effectiveness of dynamic roughness on the initial formation of the LEV. Therefore, a compromise was made to make use of the laminar flow solver to capture the effects at the separation point rather than capturing all of the flow physics downstream of the separation. In addition, attempts were made by Huebsch et al. to apply a turbulence model, but none attempted accurately captured the laminar separation point [14]. This also provides reason to include an experimental analysis to provide further reinforcement of what was observed in the CFD simulations (Figures 5 and 6).

A grid and temporal independence study were conducted at a Reynolds number of 150,000 prior to performing production runs. Due to the unsteady nature of the dynamic stall process, an angle of attack where separation is first initiated was selected as the indicator of grid independence. For these flow conditions, that occurred at an

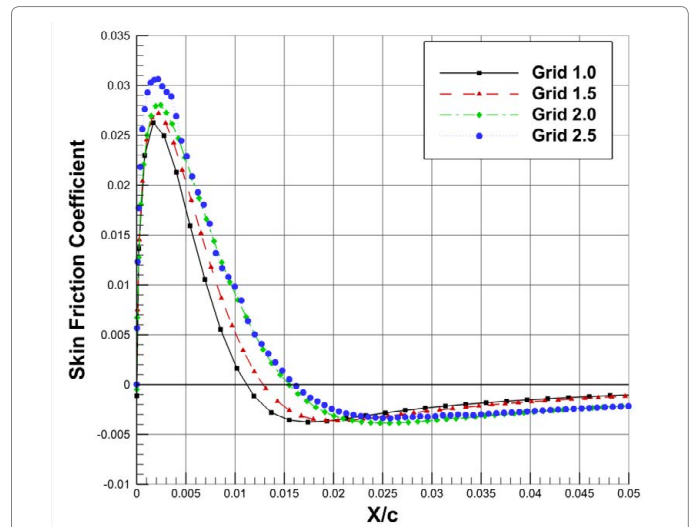


**Figure 7:** Skin friction coefficient as a function of chord location at a time corresponding to the onset of separation during a pitch-up maneuver (6.1° angle of attack), which was used for the grid independence study.

angle of attack of 6.1°. To compare separation points, the location of the zero skin friction coefficient was evaluated among the different grids. Table 1 lists the properties of each grid and plots of skin friction coefficient corresponding to chord location for each grid are shown in (Figure 7). The plot focuses on the first 5% of chord length to highlight the grid independence. Between grid 2.0 and grid 2.5 there was a difference in separation location of only 4.5%, therefore it was decided grid 2.0 was sufficient. A similar procedure was used to verify temporal independence. A typical non-dimensional time step was introduced, given in Eq. (3).

$$\Delta t^* = \frac{\Delta t U_\infty}{c} \quad (3)$$

Here,  $\Delta t^*$  is the non-dimensional time step and  $\Delta t$  is the dimensional time step used in the simulations. A time independent solution was found using a non-dimensional time step of 0.001. This non-dimensional time step also dictated that the number of time steps per dynamic roughness actuation cycle would be no less than 41. It

was shown that increasing the number of steps per dynamic roughness cycle produced no difference in results (Table 2) (Figure 7).

A true grid independence study was not completed for the three-dimensional grid due to resource limitations. A 1.8 million node grid was developed for the three-dimensional simulations. The smallest spacing along the airfoil's surface was 0.0018c and the smallest spacing normal to the airfoil's surface was 0.0002c. The span-wise spacing was a constant 0.0018c to provide adequate shape modeling of the dynamic roughness elements. Symmetry boundary conditions were used on the side faces of the domain.

## Results for Lev Control

### Experimental analysis

The primary tool used in the experimental analysis of dynamic roughness effects on LEV formation was particle image velocimetry, or PIV. PIV data were collected at a variety of flow and pitching conditions, with and without active dynamic roughness. To serve as a consistency check the relationships between LEV development, Reynolds number, and reduced oscillation frequency were evaluated and compared to the trends established in the literature. For example, previous research indicates that the Reynolds number has little effect on LEV development, while changes in reduced oscillation frequency can greatly impact the vortex development [21,22].

Reynolds number dependence was first evaluated by maintaining the reduced oscillation frequency of the airfoil constant at  $k=0.1$ . Table 2 briefly outlines the dimensional characteristics for each case. The Reynolds number range was chosen based on a combination of the expected range to be studied using computational methods, wind tunnel capabilities, and oscillation mechanism performance. As is typical in the analysis of PIV data, a series of images were used to provide an average flow field at each desired angle of attack, or a phase-averaged PIV data. This was accomplished by triggering the cameras and lasers based on the output of the absolute encoder embedded on top of the model support shaft. A total of 100 images were used to create an average velocity vector field. The use of additional images in the averaging process showed no difference in results. The frequency of oscillation of the airfoil dictated the rate at which PIV data was

collected. The maximum rate at which particle images can be acquired by the PIV system is 2.4 Hz, but if the oscillation rate was slower than this, then the PIV system would wait until the airfoil was at the correct angle of attack before acquiring a new data point (Table 3).

The results of the Reynolds number dependence study are summarized in Figure 8. Contours of the chord-wise velocity component overlaid on the velocity vector and streamlines are plotted at three different angles of attack for each Reynolds number. These angles of attack were chosen because of the formation of the LEV at this position during the pitch-up motion. The trend shown in the figure reinforces the idea that the Reynolds number has little effect on the evolution of the LEV in the Reynolds number regime studied. There may be subtle differences in circulation center or extent of recirculation region normal to the airfoil surface, but globally there was little difference among the Reynolds numbers studied. This agrees well with previous research [21,22].

A similar validation study was conducted to investigate the effects of increasing the reduced frequency, and in essence the pitching rate, on a clean airfoil. In this case, the Reynolds number was held constant at  $Re=80,000$  while PIV data were recorded at reduced frequency values of  $k=0.1$ ,  $k=0.15$ , and  $k=0.2$ . In contrast to the Reynolds number dependence, it is evident that the reduced frequency plays an important role in LEV development. With an increase in reduced frequency, LEV development was clearly delayed until higher angles of attack. Results showing this delay in LEV formation are provided in Figure 9. At an angle of attack of  $26^\circ$  and a reduced frequency of 0.1, the LEV was well established and the reattachment point was out of view of the frame. At the same angle of attack, but with an increased reduced frequency of 0.2 the LEV was just starting to develop. At a higher angle of attack of  $28^\circ$  the LEV had still not progressed to the stage seen at an angle of attack of  $26^\circ$  and at the lower reduced frequency. This result agrees well with previous LEV studies which showed the same trend of increased reduced frequency resulted in delayed LEV development to higher angles of attack. Both the Reynolds number and reduced frequency dependence studies helped to validate the experimental setup, as well as the ability for phase-averaged PIV to capture the development of the LEV (Figures 8 and 9).

Once the experimental setup and PIV analyses were consistent with past results, the next step was to evaluate the effectiveness of dynamic roughness to alter the LEV formation. A variety of flow and dynamic roughness conditions were considered, with some results that showed clear LEV delay, some with more subtle differences, and also conditions where dynamic roughness had no effect. It should be noted that the Reynolds number range shown in the experimental results does not coincide with those shown in the computational simulations, though all would be considered in the low Reynolds number regime for aerodynamic bodies. Experiments were initially conducted at similar Reynolds numbers as the computational results, but no effect due to the dynamic roughness was realized at these flow conditions in the experimental data. It was then decided to increase the Reynolds number in the experiments since the computational simulations indicated a trend that the dynamic roughness had more effect as Reynolds number was increased. This was indeed shown to be the case since conditions were found in the experimental results that showed delay of the LEV development due to the dynamic roughness. The authors suspect that the use of a laminar solver, lack of free-stream turbulence, and the neglect of inertial terms due to the pitching method in the simulations prevented the direct quantitative comparison between CFD and experiment, but similar qualitative trends are identified in both methods of investigation.

Grid	$N_s$	$N_N$	$\Delta x/c$	$\Delta y/c$	$N_{BL}$
1	103	120	0.0022	4.00E-05	39
1.5	153	180	0.0014	4.00E-05	53
2	180	206	0.001	4.00E-05	66
2.5	257	240	0.0008	7.00E-07	118

$N_s$ ≡Number of nodes along airfoil's surface.

$N_N$ ≡Number of nodes normal to airfoil's surface.

$\Delta x/c$ ≡Minimum node spacing along airfoil's surface, non-dimensionalized by chord length.

$\Delta y/c$ ≡Minimum node spacing normal to airfoil's surface, non-dimensionalized by chord length.

$N_{BL}$ ≡Number of nodes in boundary layer measured normal to airfoil surface at mid-chord at  $0^\circ$  angle of attack.

**Table 2:** Properties of the grids used in the refinement study.

Re	$U_\infty$	k	$\omega$	Motor RPM
	(m/s)		(rad/s)	
80,000	4	0.1	2.74	26.2
1,50,000	7.5	0.1	5.14	49
2,00,000	10	0.1	6.85	65.4

**Table 3:** Conditions used to observe changes in LEV development with respect to Reynolds number.

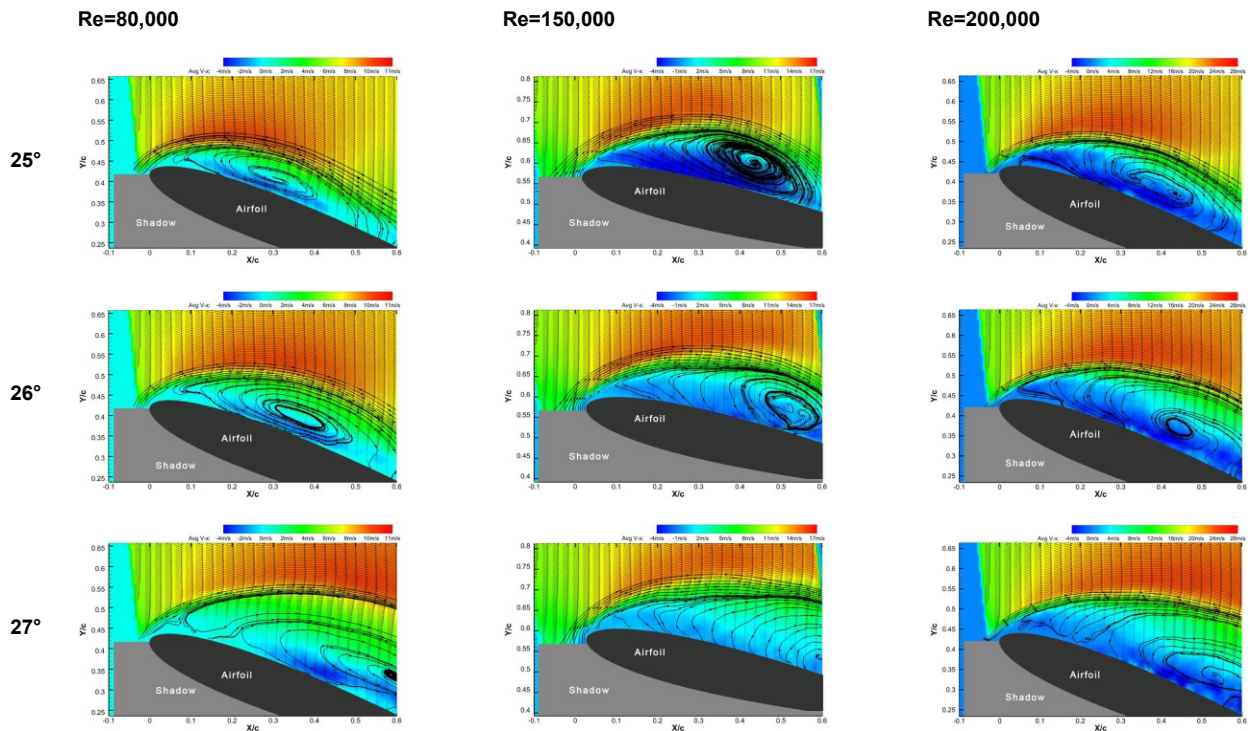


**Figure 8:** PIV results for the evolution of the LEV at varying Reynolds numbers and instantaneous angles of attack at the same reduced frequency,  $k=0.1$ , for a clean airfoil with no dynamic roughness actuation.<sup>1</sup>

<sup>1</sup>The PIV results collected at  $Re = 150,000$  were taken with a slightly different camera angle.

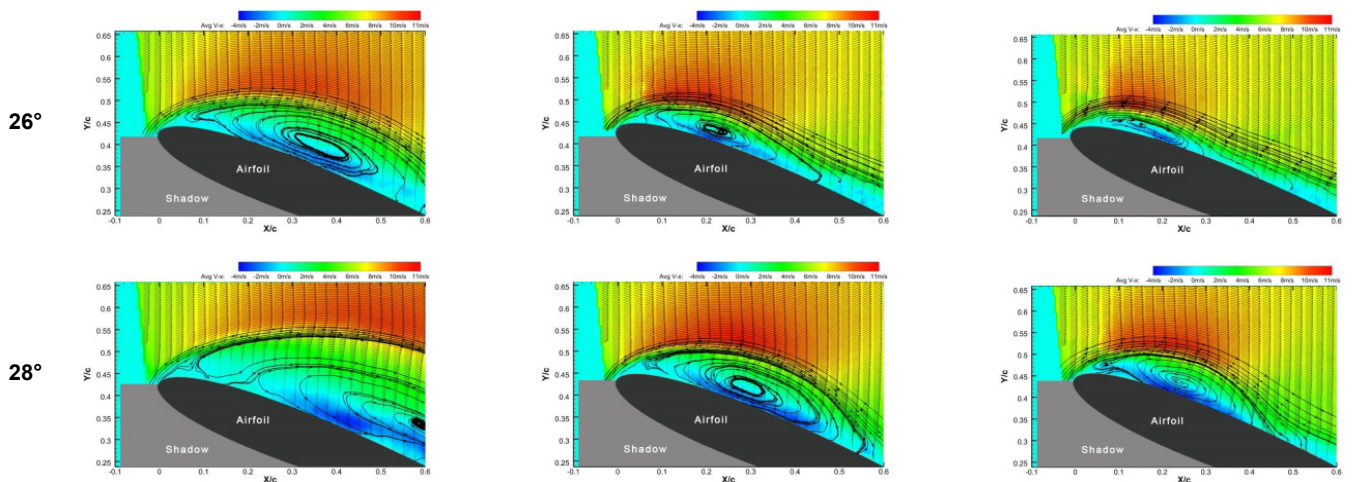


**Figure 9:** PIV results for the change in LEV formation as reduced frequency,  $k$ , is increased and Reynolds number is held constant at 80,000 for a clean airfoil with no dynamic roughness actuation.

A series of figures are provided below to illustrate the effect the dynamic roughness had on the development of the LEV. The images provide contours of chord-wise velocity magnitude, overlaid with velocity vectors and streamlines as the airfoil was in a rapid pitch up. These images clearly show the formation of a large recirculation region with separation and reattachment points. Figure 10 provides data for a Reynolds number of 80,000 and a reduced pitching frequency of  $k=0.1$ . The dynamic roughness actuation frequency was 89 Hz and the maximum amplitude was 0.301 mm (5.2% of roughness element

diameter); these dynamic roughness conditions represent the maximum capability of the dynamic roughness actuation system used in these experiments. Although there were subtle differences between the clean and dynamic roughness cases within the recirculation region, the separation and reattachment points were unaltered, as was the distance the LEV grew normal to the airfoil's surface. This was also found to be the case if the dynamic roughness actuation frequency or amplitude were reduced.

The next flow condition investigated, shown in Figure 11, was for a Reynolds number of 150,000 and a reduced pitching frequency of  $k=0.1$ . The maximum performance of the dynamic roughness actuation system provided conditions that were capable of delaying the development of the LEV. The clean airfoil exhibited the formation of the LEV at an angle of attack of  $21^\circ$ , with a separation point near the leading edge and clear reattachment downstream. At the same angle of attack for an airfoil with dynamic roughness actuated, there was no visible flow separation and the flow remained attach along the surface of the airfoil. Even at an angle of attack of  $22^\circ$  there was still no apparent LEV development. As the angle of attack was increased separation occurred, although the development of the LEV appears to progress differently when compared to the clean airfoil. As can be seen

in the figure, during the pitch-up process for the dynamic roughness case there was no large LEV development over the upper surface of the airfoil. The flow appeared separated from the surface, with no reattachment as was seen in the clean airfoil. Also, the recirculation region appeared to remain in closer proximity to the airfoil surface when dynamic roughness was actuated. This was most likely due to small vortices that were shed and convected downstream during the pitch-up process, instead of the development of a large LEV, and the consequence of phase averaging multiple vector fields to produce an average flow field. Further study should be completed, ideally involving force and pitching moment measurements, to identify whether this altered LEV development process mitigates the rapid change in pitching moment associated with the LEV shedding downstream.

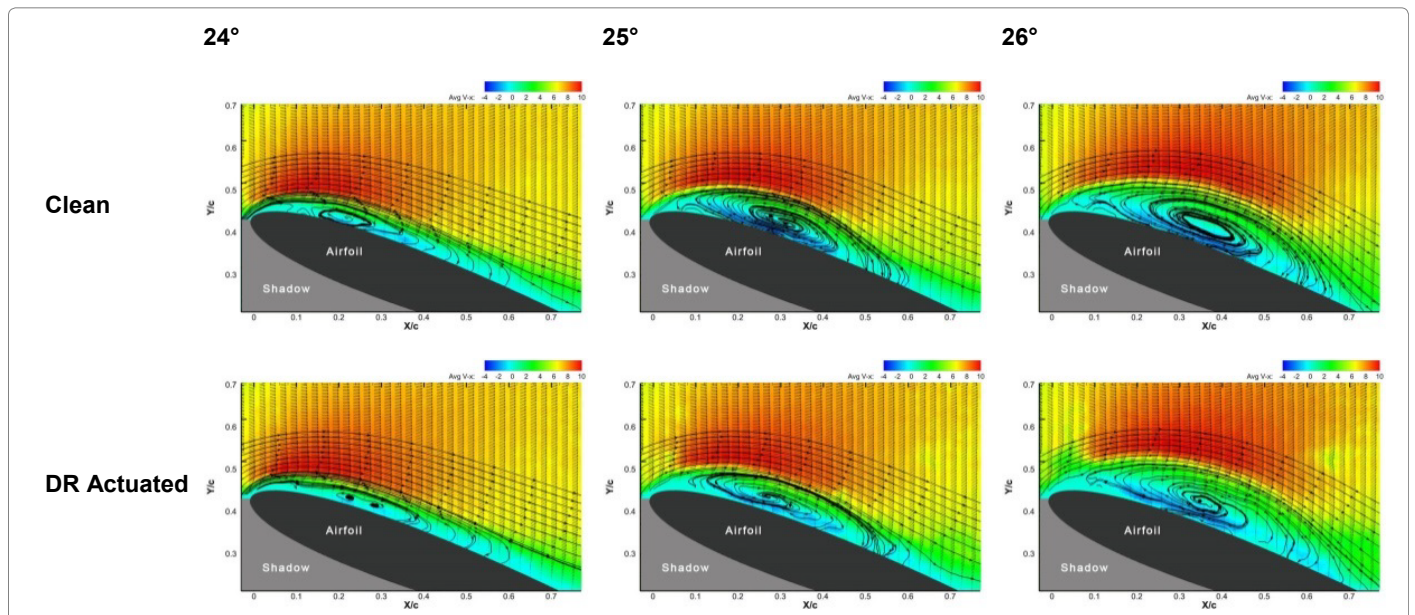


Figure 10: Contours of chord-wise velocity magnitude overlaid with velocity vectors and streamlines at  $Re=80,000$  and  $k=0.1$  for both clean and dynamic roughness cases during rapid pitch up. The DR conditions include: 89 Hz actuation frequency and 0.301 mm maximum amplitude.

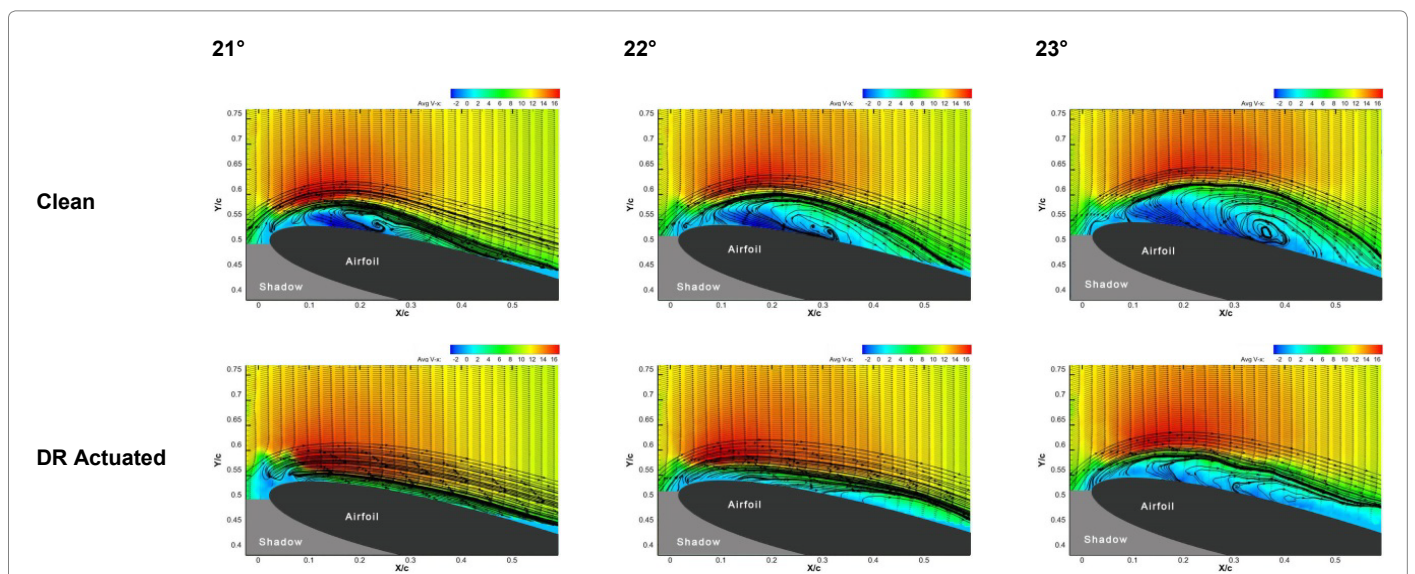


Figure 11: Contours of chord-wise velocity magnitude overlaid with velocity vectors and streamlines at  $Re=150,000$  and  $k=0.1$  for both clean and dynamic roughness cases during rapid pitch up. The DR conditions include: 89 Hz actuation frequency and 0.301 mm maximum amplitude.

The Reynolds was increased again to a value of 200,000 while keeping the reduced pitching frequency the same,  $k=0.1$ . Again, the maximum capability of the dynamic roughness actuation system was required to produce any alteration in the LEV development process. At this flow condition the LEV development was delayed, but not as clearly and robustly as at a Reynolds number of 150,000. Figure 12 highlights that in the dynamic roughness case the location of leading edge separation is shifted aft when compared with the clean airfoil at the same angle of attack. This phase averaged data also exhibits a “stretched” LEV region, with no clear reattachment point visible. It is hypothesized this is due to vortices being shed as the LEV grows. This vortex shedding is not captured by the phase averaged PIV, but may cause the “stretching” effect shown here. It is also important to note that the dynamic roughness actuation system was operated at its maximum performance to produce the results shown. It is not unreasonable to assume that more robust delay of the LEV development at the higher Reynolds number could be realized with a more capable actuation system (Figures 10–12).

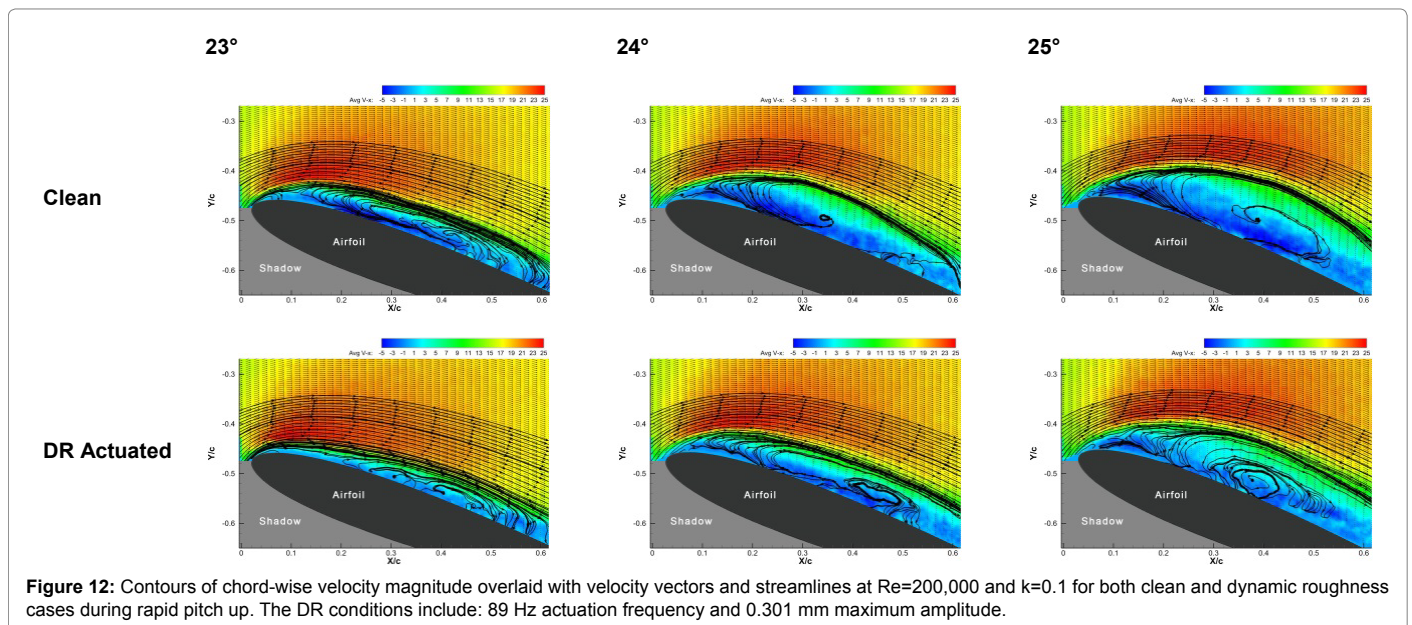
### Computational results

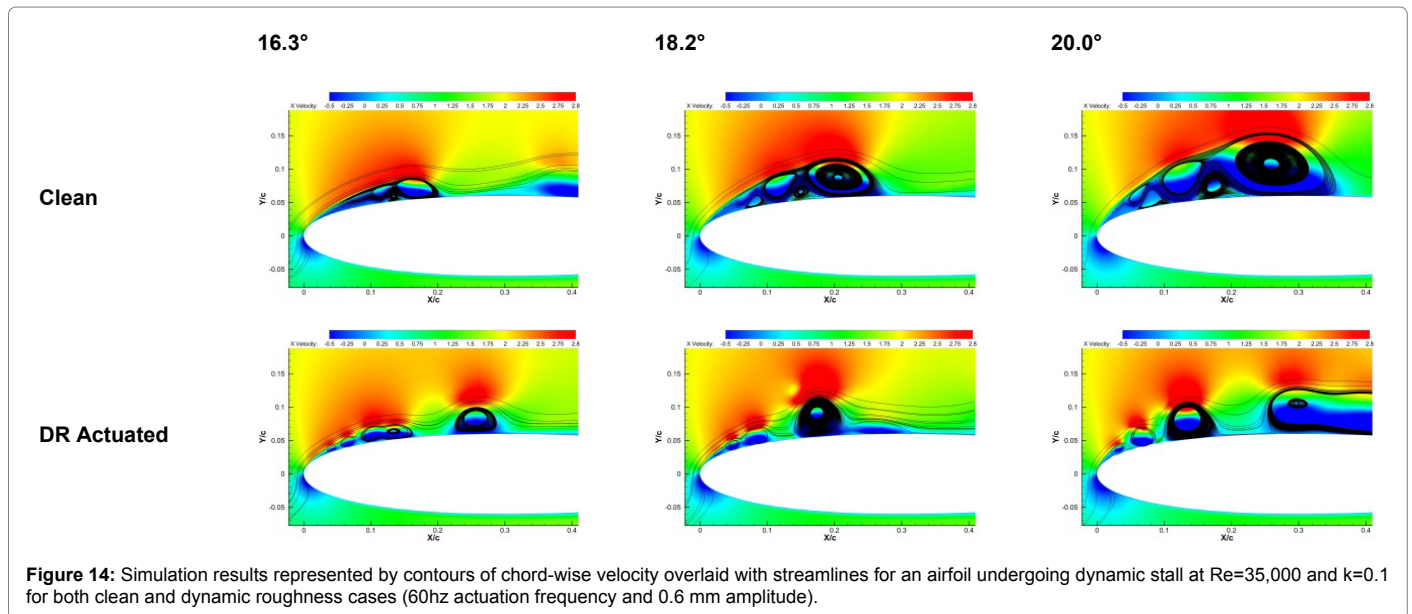
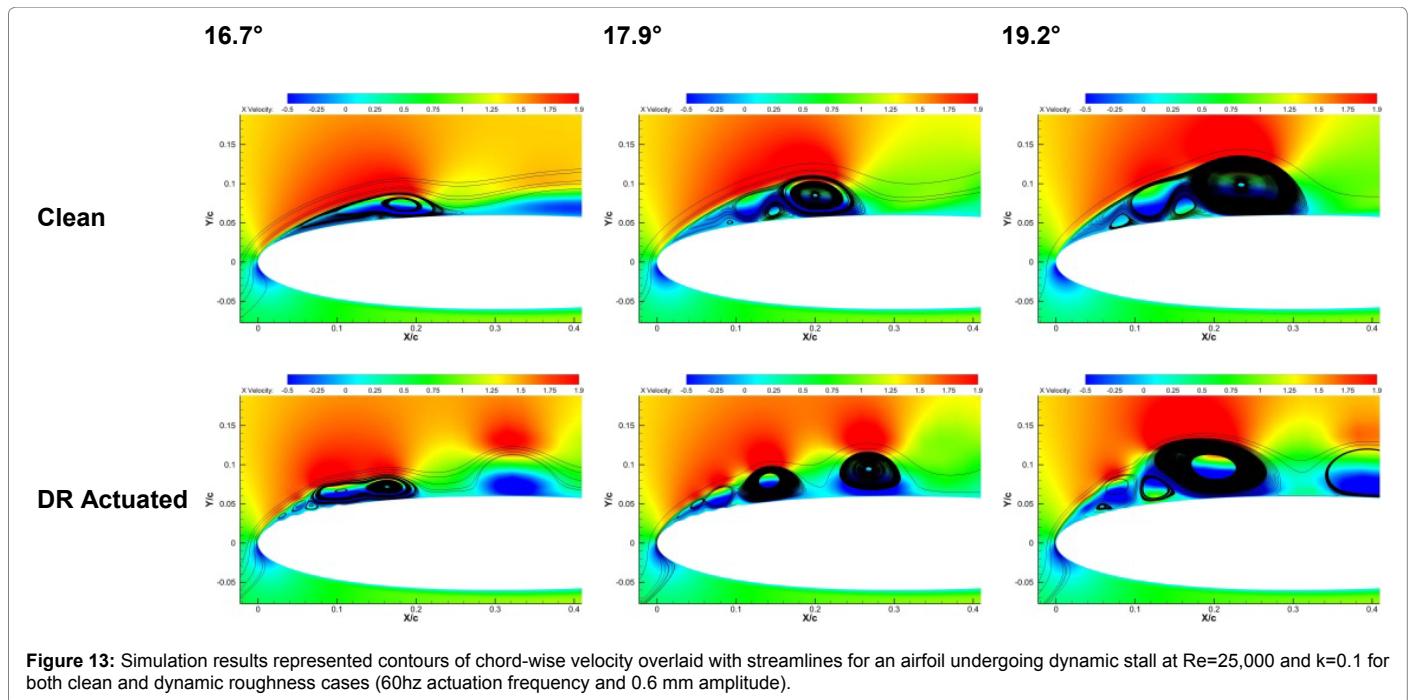
A computational approach was also used in the investigation of dynamic roughness effects on LEV formation. As noted in section 3, it was decided to apply a laminar flow solver for the CFD simulations in this work. There were two primary reasons for this selection, one of which was properly capturing certain flow physics and the other being available computational resources. For leading edge separation phenomena, the boundary layer is typically laminar in the region of the separation point. Based on past work, it was decided that a laminar solver would be more appropriate to capture the original separation event. The authors do fully recognize that the flow transitions to turbulent in the reattachment process and remains turbulent downstream. However, applying a turbulence model to the flow field can be detrimental to the boundary layer separation process. Gall [23] conducted research on leading-edge separation bubbles and found that the application of the  $k-\epsilon$  turbulence model fully suppressed the formation of the leading-edge bubble. Admittedly the formation of the dynamic stall vortex is a more robust process than the laminar separation bubble and application of a turbulence model would not

likely fully suppress this formation, but there was concern that it would alter the boundary layer separation physics, particularly with respect to the dynamic roughness actuation. Therefore, the laminar solver was used to take a qualitative look at the effects of dynamic roughness on the formation of the LEV and identify any potential trends among some of the known first-order parameters such as dynamic roughness actuation frequency and amplitude.

After applying dynamic roughness to a variety of flow conditions, it appeared that the effectiveness of dynamic roughness was greater as Reynolds number was increased. For consistency, the dynamic roughness element diameters were kept constant at 2% chord length. Figure 13 through Figure 15 compare simulated pitching airfoils with and without dynamic roughness actuated for three different Reynolds numbers. At a Reynolds number of 25,000 not only does dynamic roughness not delay LEV development, but it actually hastened vortex formation. This could also prove to be beneficial in some cases of “controlling” the LEV development. As Reynolds number was increased to 35,000, additional effect from dynamic roughness was apparent. As shown in Figure 13, the LEV region with dynamic roughness actuated did not extend as far downstream or normal to the airfoil surface as was shown in the clean airfoil case. It appeared vortices were shed earlier in the LEV development process, leading to a smaller recirculation region. The effectiveness of dynamic roughness was much more pronounced at a Reynolds number of 50,000, clearly producing a significant delay in the development of the LEV. Again, it appeared small sized vortices were shed downstream for the dynamic roughness case, resulting in a delay of LEV development to higher angles of attack. This also seems to correspond to the experimental results stated previously (Figures 13-15).

Studies on the effect of dynamic roughness amplitude and frequency were also conducted. The free stream conditions were kept constant with a Reynolds number of 50,000 and a reduced frequency of 0.1. The dynamic roughness actuation frequency was first held constant at 60 Hz, since this frequency showed the most significant delay in LEV development, while the maximum amplitude was reduced by half. The original amplitude was 10% of the dynamic roughness element diameter (0.5842 mm). Figure 16 compares the two different amplitude settings along with the clean airfoil results. Even at half the



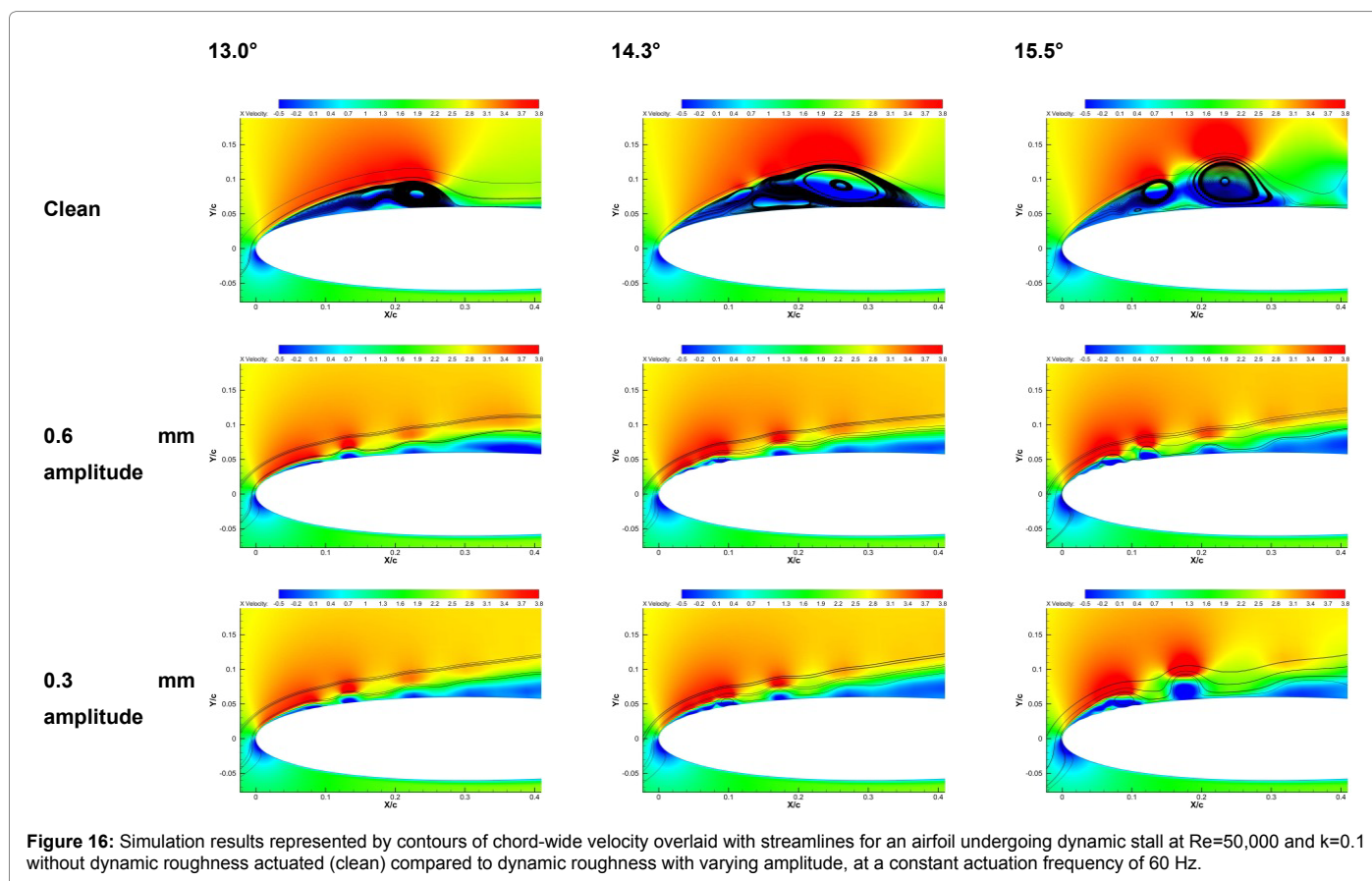
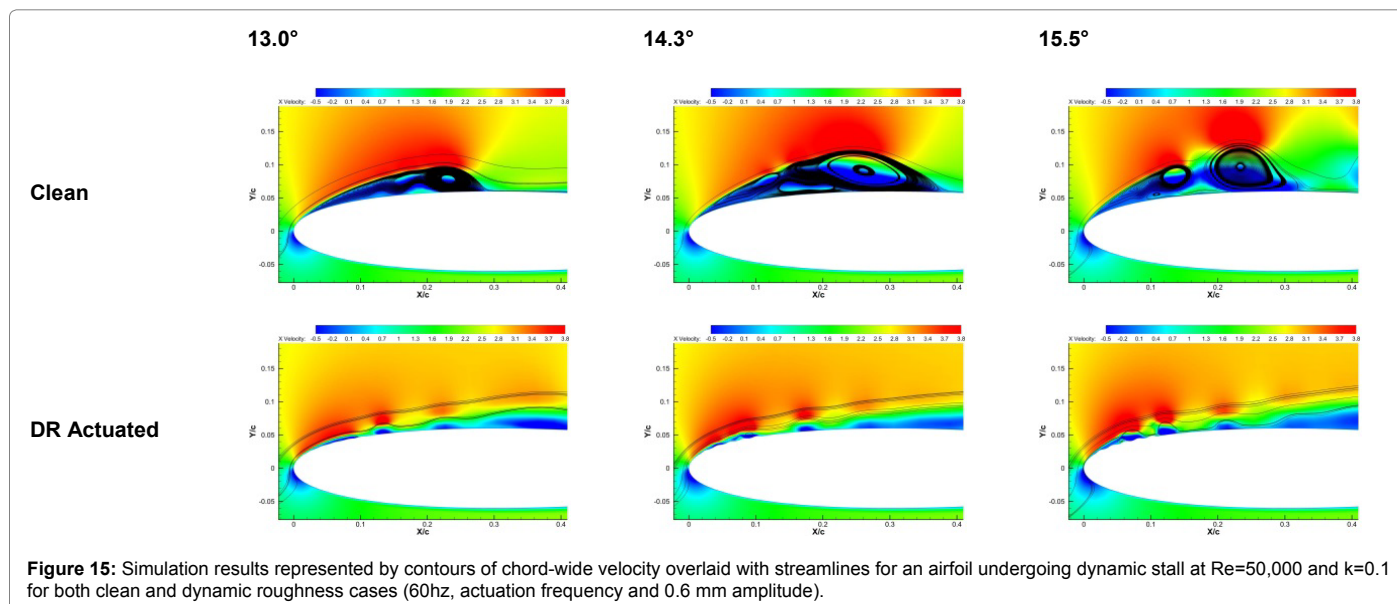


amplitude, LEV development was significantly delayed by the dynamic roughness, with both amplitude settings producing a similar impact on the LEV development. At an angle of attack of  $15.5^\circ$ , the first primary vortex appeared to begin to shed downstream in the clean case. At the same angle of attack with dynamic roughness there is no coherent LEV formation for both amplitude settings. This demonstrated the robustness of dynamic roughness to delay LEV formation at small amplitudes, and perhaps its ability to function at off-design conditions (Figure 16).

A similar parametric approach was used to evaluate dynamic roughness actuation frequency dependencies at the same  $Re=50,000$ . Figure 17 compares results provided by dynamic roughness actuated at

90 Hz to those with an actuation frequency of 20 Hz (previous results were at 60 Hz), keeping the maximum amplitude constant at 10% of the roughness element diameter. Even at the lower dynamic roughness frequency the LEV development is clearly delayed, but the higher frequency shows a more significant suppression of the LEV, similar to the previous results when the actuation frequency was at 60 Hz (Figure 17).

An interesting observation was made utilizing the computational results that differed from past observations for dynamic roughness flow control at static angles of attack. For the dynamic pitch up flow regime there was a limited range of dynamic roughness frequencies that produced the greatest delay in LEV development. In previous work



done by Huebsch et al. [14] concerning the ability of dynamic roughness to eliminate the laminar separation bubble on an airfoil at a static angle of attack it was found that a minimum frequency was required for flow control. With Reynolds number and maximum amplitude held constant, applied frequencies above this minimum value resulted in a similar ability to eliminate the laminar separation bubble with no negative effects. In the current study of dynamic pitch up, higher

frequencies eventually reduce the effectiveness of dynamic roughness to delay LEV development. Figure 18 is provided to illustrate this observation. Here the free-stream conditions and dynamic roughness amplitude were held constant ( $Re=50,000$ ,  $k=0.1$ , DR amplitude = 2% diameter) while the dynamic roughness frequency was varied (20 Hz, 60 Hz, 180 Hz). The dynamic roughness frequency of 60 Hz provides the greatest delay in LEV development. This indicates for this type of

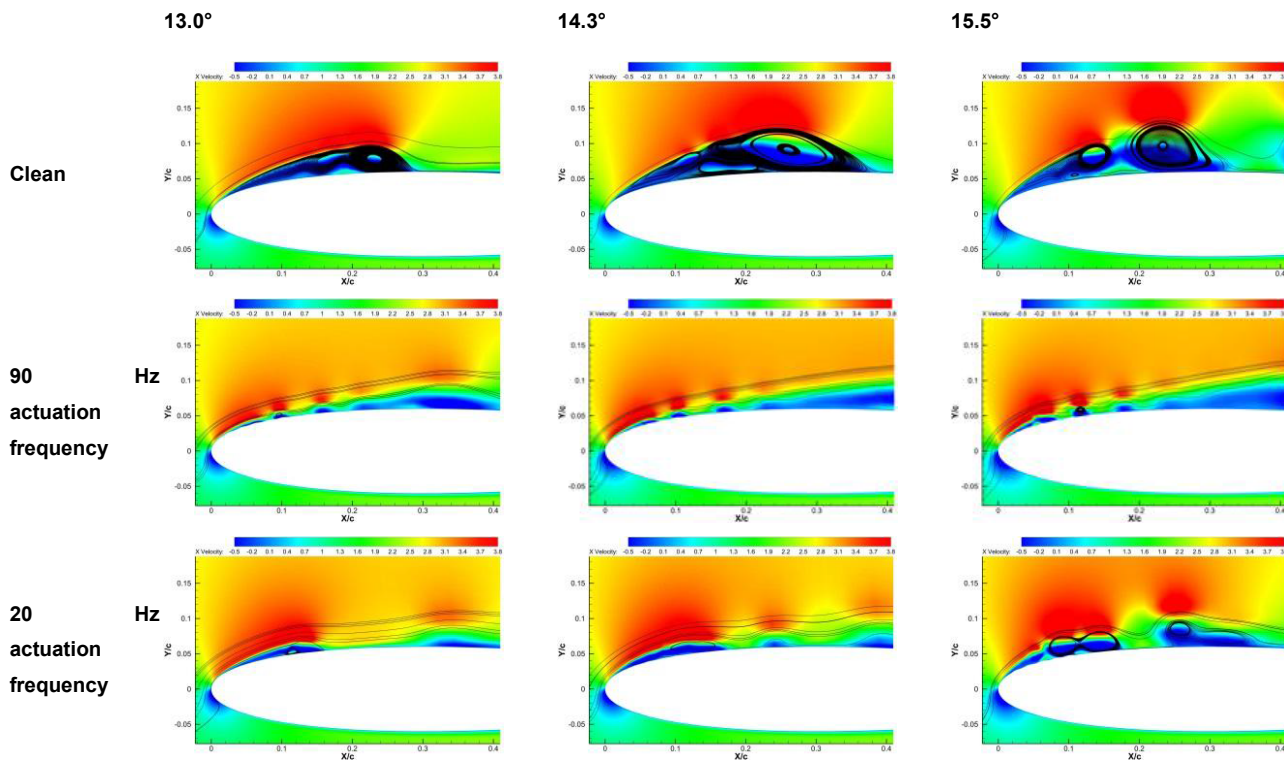


Figure 17: Simulation results represented by contours of chord-wide velocity overlaid with streamlines for an airfoil undergoing dynamic stall at  $Re=50,000$  and  $k=0.1$  without dynamic roughness actuated (clean) compared to dynamic roughness at varying actuation frequencies and a maximum amplitude of 10% of the roughness diameter.

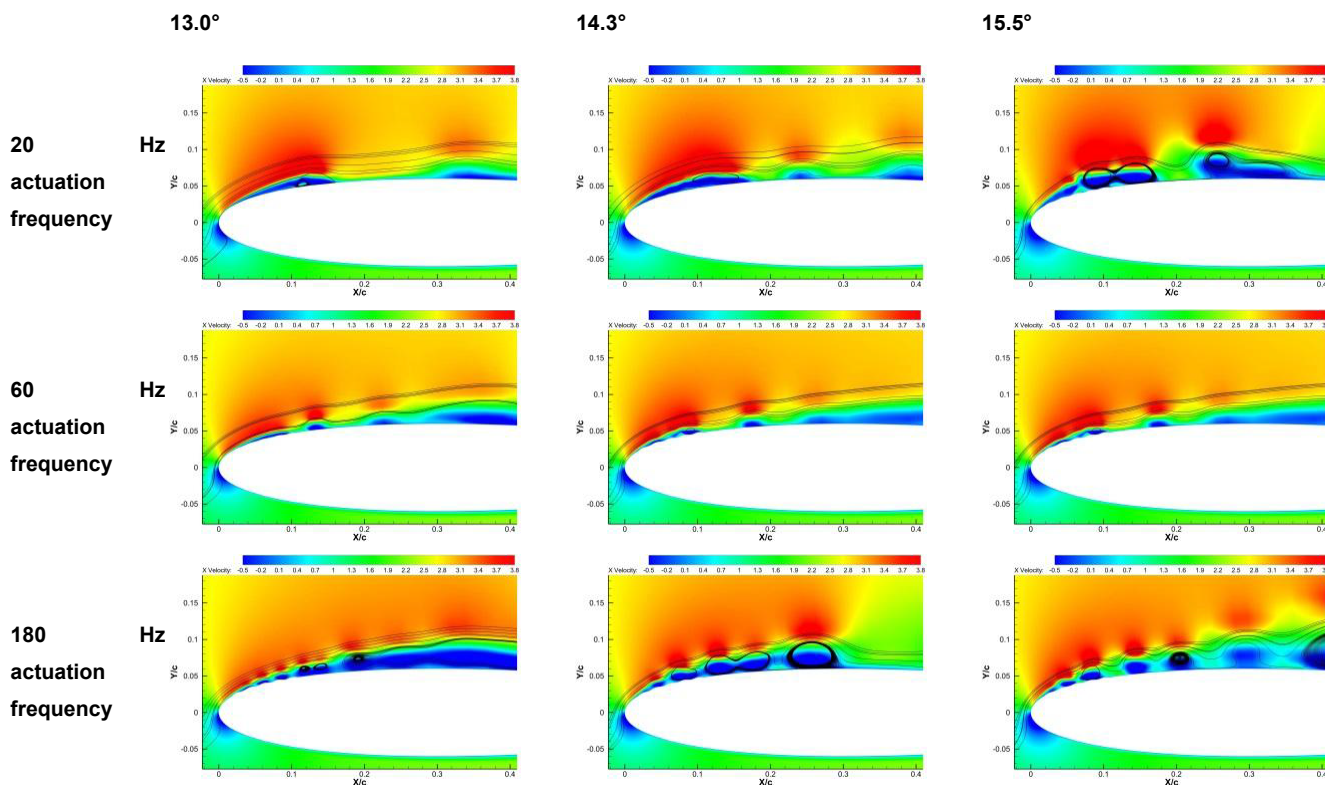


Figure 18: Simulation results represented by streamlines colored by vorticity magnitude for an airfoil undergoing dynamic stall at  $Re=50,000$  and  $k=0.1$  with dynamic roughness actuation at constant amplitude (10% element diameter), but with an actuation frequency of 20 Hz, 60 Hz, and 180 Hz, respectively.

unsteady separation there is a bandwidth of frequencies that provide flow control, rather than a threshold frequency (Figure 18).

Three-dimensional computational cases were also explored to investigate effects that may arise due to span-wise flow both over the wing surface as well as around a three-dimensional roughness element. Since a uniformly extruded airfoil shape was modeled there were no tip effects or sweep to produce significant span-wise flow. Delay of LEV development due to dynamic roughness in three-dimensional simulations was similar to the results gathered by two-dimensional simulations. Figure 19 provides further validation that dynamic roughness can delay LEV formation and that three-dimensional simulations correspond well to two-dimensional simulations (Figure 19).

An iso-surface plot was developed and is shown in Figure 20. The plot consists of an iso-surface of a single vorticity magnitude value, contoured by the chord-wise velocity component. This type of plot shows how the vorticity was altered by the dynamic roughness, and predominantly by the first two rows of dynamic roughness elements. The first row develops a very short bulge region, which accelerates flow between adjacent elements. This accelerated flow then creates a long bulge region that seems to remain unaltered by the aft dynamic

roughness elements. This correlates well to the numerical work done by Rothmayer, et al. [24,25], which concluded the “largest contributors to flow control for laminar separation on airfoils at static angles of attack are the start and end of the dynamic roughness field”. This is due to the first dynamic roughness elements producing all of the acceleration with the middle of the dynamic roughness field producing no local acceleration or deceleration. A deceleration is then initiated by the termination of the dynamic roughness field (Figure 20).

Although the CFD visualization plots provide evidence that DR has the ability to delay the LEV formation, it should be shown this delay is beneficial in some way. To this end, Figure 21 is presented to show the lift-to-drag comparison of an airfoil pitching at  $Re=50,000$  and  $k=0.1$ , with and without dynamic roughness actuation. The general oscillations in the data are due to vortices being shed as the airfoil was pitched-up. The blue box highlights the portion of the pitch-up maneuver in which the LEV was visually delayed during dynamic roughness actuation, refer to Figure 15. At approximately  $13^\circ$  AOA, a spike in the lift-to-drag ratio was present on the clean airfoil. This corresponded with the start of the LEV formation, which produced a region of accelerated fluid near the leading edge, increasing lift with a relatively small increase in drag. As this vortex continued to grow the drag that was associated with its growth began to outweigh the benefit of the accelerated fluid, thus the decrease in lift-to-drag ratio. In the same region on an airfoil where dynamic roughness was utilized the lift-to-drag ratio became elevated at a lower angle of attack and remained elevated for a longer duration of the pitch-up maneuver, increasing the lift-to-drag ratio by approximately 60% at  $15^\circ$  AOA. This provides preliminary evidence that delaying the LEV formation can increase airfoil efficiency. Another significant detail provided from Figure 21 is that there seemed to be no degradation in lift-to-drag ratio at lower angles of attack when dynamic roughness was actuated, but before LEV development was initiated. This can be a significant benefit for any device that may be operated at off-design conditions (Figure 21).

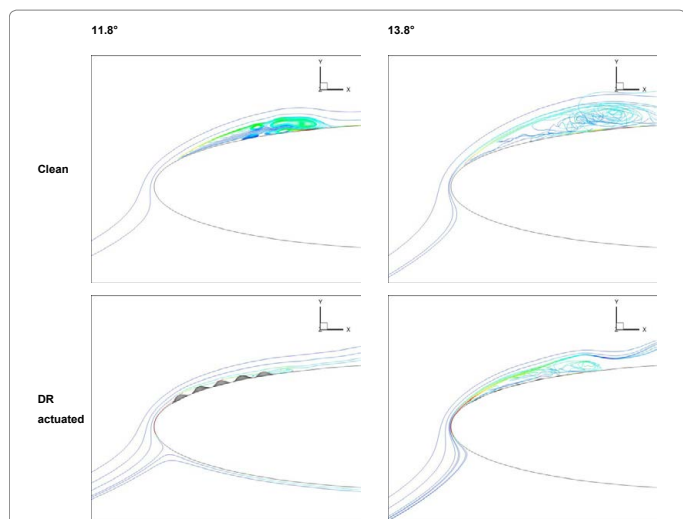


**Figure 19:** Streamlines colored by vorticity magnitude of three-dimensional simulation results for a clean airfoil and an airfoil with dynamic roughness actuation, respectively. The flow conditions were:  $Re=50,000$  and  $k=0.1$ . The dynamic roughness conditions were: actuation frequency=60 Hz and maximum amplitude=10% roughness element diameter.

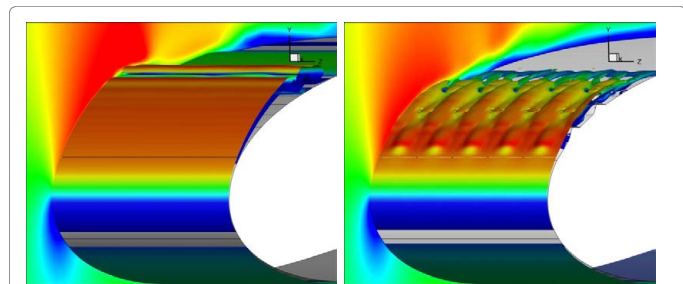


**Figure 20:** Iso-surface of a single vorticity magnitude contoured by chord-wise velocity component for a clean airfoil at  $11.8^\circ$  angle of attack and an airfoil with actuated dynamic roughness at the same angle of attack, respectively. The flow conditions were:  $Re=50,000$  and  $k=0.1$ . The dynamic roughness conditions were: actuation frequency=60 Hz and maximum amplitude=10% roughness element diameter.

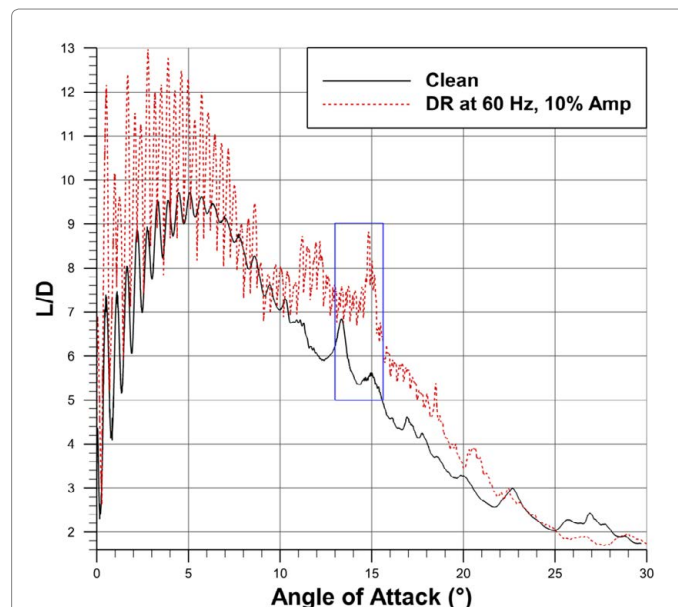


**Figure 21:** Ratio of lift-to-drag for a clean airfoil and for an airfoil in which dynamic roughness was actuated at a frequency of 60 Hz and an amplitude of 0.6 mm for an airfoil pitching at  $k=0.1$  and  $Re=50,000$ . The blue box highlights the portion of the pitch-up maneuver in which the LEV is visibly delayed for the dynamic roughness case.

## Conclusions

Experimental and computational studies were conducted to evaluate the effectiveness of dynamic roughness to alter the development of the LEV encountered on an airfoil undergoing dynamic stall. Both the experiments and simulations were performed on a model NACA 0012 airfoil at a variety of relatively low Reynolds numbers. Numerical solutions were carried out by the commercial code FLUENT, which was amended by way of UDFs to simulate moving walls (dynamic roughness elements) as well as to simulate a pitching airfoil. Experimental results were provided by PIV.

The results of this research effort indicate dynamic roughness has the ability to significantly delay the development of the LEV in the Reynolds number and reduced pitching frequency ranges studied. Cases were shown where dynamic roughness had significant effect on the LEV development, as well as cases where dynamic roughness had little to no effect. The computational simulations showed a trend in which effectiveness of dynamic roughness increases with Reynolds number. A more robust dynamic roughness actuation system is needed to provide experimental evidence of the same trend. In addition, dynamic roughness was able to delay LEV development at reduced amplitudes, highlighting the ability to perform in off-design conditions. It was also shown that dynamic roughness actuation frequency plays a more important role than dynamic roughness actuation amplitude and that there is no minimum frequency “threshold” as was found in prior uses of dynamic roughness at static angles of attack. Frequencies outside a certain range lose the ability to significantly delay LEV development. Three-dimensional simulation results compared well with two-dimensional simulations results. The agreement between two-dimensional simulations and three-dimensional simulations also provides evidence that two-dimensional simulations suffice when studying simple airfoil geometries, which would benefit parametric studies to find a range of dynamic roughness properties required for significant LEV development delay. Three-dimensional simulation results also hinted that the majority of the “work” done to delay LEV development is done by the first two rows of dynamic roughness elements. Applying a laminar solver also proved to be appropriate in the Reynolds number regime studied. This limitation is complemented by the experimental analysis.

## Acknowledgements

This work was funded, in part, by NASA Grant NNX09AW07A.

## References

- Muijres FT, Johansson LC, Barfield R, Wolf M, Spedding GR et.al. (2008) Leading-Edge Vortex Improves Lift in Slow-Flying Bats. *Science* 319: 1250-1253.
- Pournazeri S, Segre P, Princevac M, Altshuler D (2012) Hummingbirds Generate Bilateral Vortex Loops During Hovering: Evidence from Flow Visualization. *Experiments in Fluids* 54: 1.
- Fuchiwaki M, Kuroki T, Tanaka K, Tabata T (2013) Dynamic Behavior of the Vortex Ring Formed on a Butterfly Wing. *Experiments in Fluids* 54: 1.
- Geissler W, Haselmeyer H (2006) Investigation of Dynamic Stall Onset. *Aerospace Sci Technol* 10: 590-600.
- Freytmuth P, Jackson S, Bank W (1988) Toward Dynamic Separation Without Dynamic Stall. *Exp Fluids* 7: 187-196.
- Karim MA, Acharya M (1994) Suppression of Dynamic-Stall Vortices Over Pitching Airfoils by Leading-Edge Suction. *AIAA J* 32: 1647-1655.
- Carr L, McAlister K (1983) The Effect of a Leading-Edge Slat on the Dynamic Stall of an Oscillating Airfoil. *AIAA Paper* 85: 25-33.
- Chandrasekhara M, Martin PB, Tung C (2004) Compressible Dynamic Stall Control Using a Variable Droop Leading Edge Airfoil. *J Aircr* 4: 862-869.
- Greenblatt D (2010) Active Control of Leading-Edge Dynamic Stall. *International Journal of Flow Control* 2: 21-38.
- Post ML and Corke TC (2006) Separation Control Using Plasma Actuators: Dynamic Stall Vortex Control on Oscillating Airfoil. *AIAA J* 44: 3125-3135.
- Dearing S, Lambert S, Morrison J (2007) Flow Control with Active Dimples. *Aeronaut J* 111: 705-714.
- Grosjean C, Lee GB, Hong W, Tai YC, Ho C (1998) Micro Balloon Actuators for Aerodynamic Control. The 11th Annual International Workshop on Micro Electro Mechanical Systems.
- Huebsch WW (2006) Two-Dimensional Simulation of Dynamic Surface Roughness for Aerodynamic Flow Control. *Journal of Aircraft* 43: 353-363.
- Huebsch WW, Gall PD, Hamburg SD, Rothmayer AP (2012) Dynamic Roughness as a Means of Leading-Edge Separation Flow Control. *J Aircr* 49: 108-115.
- Grager T, Rothmayer AP, Huebsch WW, Hu H (2012) Low Reynolds Number Airfoil Stall Suppression with Dynamic Roughness, 6th AIAA Flow Control Conference. Fluid Dynamics and Co-located Conferences. American Institute of Aeronautics and Astronautics.
- Lian Y (2010) Blockage Effects on the Aerodynamics of a Pitching Wing. *AIAA J* 48: 2731-2738.
- Abbot H, von Doenhoff AE (1959) *Theory of Wing Sections*, New York: Dover Publications Inc, USA.
- Martin JM, Empey RW, McCroskey WJ, Caradonna FX (1974) An Experimental Analysis of Dynamic Stall on an Oscillating Airfoil. *Journal of the American Helicopter Society* 19: 26-32.
- McCroskey WJ, Carr LW, McAlister KW (1976) Dynamic Stall Experiments on Oscillating Airfoils. *AIAA Journal* 14: 57-63.
- Uncertainty Analysis Particle Image Velocimetry. International Towing Tank Conference 2008.
- Akbari MH, Price SJ (2003) Simulation of Dynamic Stall for a NACA 0012 Airfoil Using a Vortex Method. *J Fluids and Struct* 17: 855-874.
- Jones and Babinsky H (2011) Reynolds Number Effects on Leading Edge Vortex Development on a Waving Wing. *Exp Fluids* 51: 197-210.
- Gall PD (2010) A Numerical and Experimental Study of the Effects of Dynamic Roughness on Laminar Leading Edge Separation, PhD Dissertation, West Virginia University, USA 71:169.
- Rothmayer P, Huebsch WW (2011) On the Modification of Laminar Boundary Layers Using Unsteady Surface Actuation, 6th AIAA Theoretical Fluid Mechanics Conference. Fluid Dynamics and Co-located Conferences. American Institute of Aeronautics and Astronautics.
- Rothmayer P, Huebsch WW (2014) Control of Laminar Separation on Airfoils Using Dynamic Roughness, 7th AIAA Flow Control Conference. AIAA Aviation, American Institute of Aeronautics and Astronautics.